

A comparison of fixation and immunofluorescence protocols for successful reproducibility and improved signal in human left ventricle cardiac tissue

Matthew Taper^{1,2}  | Glenn Carrington³ | Michelle Peckham³  | Sean Lal^{1,2,4} | Robert D. Hume^{1,2} 

¹Faculty of Medicine and Health, School of Medical Sciences, The University of Sydney, Sydney, Australia

²Centre for Heart Failure and Diseases of the Aorta, The Baird Institute, Sydney, Australia

³Faculty of Biological Sciences, Astbury Centre for Structural Biology and the School of Molecular and Cellular Biology, University of Leeds, Leeds, UK

⁴Department of Cardiology, Royal Prince Alfred Hospital, Sydney, Australia

Correspondence

Robert D. Hume and Sean Lal, Faculty of Medicine and Health, School of Medical Sciences, The University of Sydney, Sydney, Australia.

Email: robert.hume@sydney.edu.au; sean.lal@sydney.edu.au

Funding information

R.T. Hall Trust; The Baird Institute

Abstract

Immunohistochemistry (IHC) and immunofluorescence (IF) are crucial techniques for studying cardiac physiology and disease. The accuracy of these techniques is dependent on various aspects of sample preparation and processing. However, standardised protocols for sample preparation of tissues, particularly for fresh-frozen human left ventricle (LV) tissue, have yet to be established and could potentially lead to differences in staining and interpretation. Thus, this study aimed to optimise the reproducibility and quality of IF staining in fresh-frozen human LV tissue by systematically investigating crucial aspects of the sample preparation process. To achieve this, we subjected fresh-frozen human LV tissue to different fixation protocols, primary antibody incubation temperatures, antibody penetration reagents, and fluorescent probes. We found that neutral buffered formalin fixation reduced image artefacts and improved antibody specificity compared to both methanol and acetone fixation. Additionally, incubating primary antibodies at 37°C for 3 h improved fluorescence intensity compared to the commonly practised 4°C overnight incubation. Furthermore, we found that DeepLabel, an antibody penetration reagent, and smaller probes, such as fragmented antibodies and Affimers, improved the visualisation depth of cardiac structures. DeepLabel also improved antibody penetration in CUBIC cleared thick LV tissue fragments. Thus, our data underscores the importance of standardised protocols in IF staining and provides various means of improving staining quality. In addition to contributing to cardiac research by providing methodologies for IF, the findings and processes presented herein also establish a framework by which staining of other tissues may be optimised.

KEYWORDS

heart, human, immunofluorescence, immunohistochemistry, immunostaining, left ventricle, microscopy, optimisation

This is an open access article under the terms of the [Creative Commons Attribution](https://creativecommons.org/licenses/by/4.0/) License, which permits use, distribution and reproduction in any medium, provided the original work is properly cited.

© 2024 The Author(s). *Journal of Microscopy* published by John Wiley & Sons Ltd on behalf of Royal Microscopical Society.

1 | INTRODUCTION

Immunohistochemistry (IHC) and immunofluorescence (IF) staining are essential laboratory techniques that provide spatial information. Through the use of probes targeting an antigen of interest, IHC/IF can ascertain the precise distribution, location, and quantity of proteins or molecules of interest in both cells and tissues. These techniques are pivotal in dissecting the complexities of cardiac physiology and pathology, as they enable insights into the mechanisms underlying cardiac development and disease.^{1,2} Such detailed knowledge is vital for developing targeted treatments and understanding the progression of cardiac diseases. However, attaining high-quality, artefact-free images is dependent on optimised sample preparation.^{3,4}

Tissue biobanks for human samples are present throughout the world and are commonly employed to study health and disease.^{5–8} Historically, these clinical samples have been preserved either as formalin-fixed paraffin-embedded blocks or in liquid nitrogen.⁹ In either case, these samples can be sectioned and used for microscopy, however, standardised protocols for the preparation of fresh-frozen human cardiac tissue are lacking. Our study therefore focuses on comparing key aspects of fresh-frozen human cardiac tissue IF techniques, enhancing their usability for microscopic analysis.

A major challenge in IF is the artefactual variability that can occur within the same sample and across different experiments.^{10–12} This variation can lead to the misinterpretation of results when discerning the expression and localisation of proteins in cardiac tissues. Differences in fixation protocols, antibody incubation temperatures, and laboratory conditions can all contribute to discrepancies in staining patterns, intensity, and ultimately, the conclusions drawn from experiments.³ Fixatives stabilise the tissue architecture and preserve the proteins of interest in their native state, which is essential for accurate antigen detection, however, different fixatives can alter antigen accessibility and visibility to varying degrees.⁴ Similarly, the incubation temperature of antibodies is another critical parameter that can affect immunolabelling results.¹³ Collectively, these steps are foundational in obtaining high-quality images that can reveal the detailed localisation of proteins within cardiac tissue.

Effective antibody penetration is critical for optimal imaging of deep structures. Historically, antibody penetration has been facilitated by the permeabilisation of cellular membranes by solvents or detergents.⁴ In thick or densely packed tissue sections such as cardiac specimens, conventional permeabilisation techniques are often inadequate, resulting in suboptimal visualisation of deeper structures and diminished fluorescence intensity.¹⁴ This challenge

is not unique to cardiac tissue and has led to the development of reagents such as DeepLabel, which have been specifically designed to improve antibody penetration.^{15,16} Furthermore, smaller probes have been developed, which, due to their size, facilitate enhanced tissue penetration.¹⁷ These include fragmented antibodies (Fabs) lacking at the fragment crystallisable (Fc) region, and Affimers, small (~12 kDa) nonantibody binding proteins isolated to proteins of interest through phage display, approximately ten times smaller than conventional antibodies.^{18–20} Nevertheless, the effectiveness of these reagents and tools in improving antibody penetration of human cardiac tissue has yet to be tested.

In choosing a sample for our study, we considered the clinical, translational relevance of our potential findings. The left ventricle (LV) is the chamber of the heart that pumps blood into the systemic circulation, thereby supplying the body with necessary nutrients and oxygen. Dysfunction of the LV is a common feature across a range of pathologies, including heart failure and ischemic heart disease. Importantly, both pathologies primarily affect middle-aged to older individuals.^{21,22} Thus, in our study, we selected a disease-free, middle-aged adult LV sample to compare optimal cardiac IF parameters that improve reproducibility, enhance fluorescent signal, and minimises artefacts or nonspecific staining. Specifically, we investigated different fixatives, incubation temperatures and antibody penetration methodologies, in both 15µm tissue sections and cleared tissue fragments (approximately 5 mm × 2 mm). The findings presented here provide a systematic comparison of various immunolabelling protocols on LV tissue sections.

2 | METHODS

2.1 | Human left ventricle tissue

Human left ventricle (LV) samples were taken from a single donor heart (54-year-old male) from the Sydney Heart Bank (SHB) at The University of Sydney. As with all SHB donor hearts, this heart that was due for transplant was instead pre-mortem collected for research with the informed written consent from the family or guardian of the organ donor due to nonclinical reasons complicating the transplantation process at the time of death, such as logistical complications, immune incompatibility, or size mismatch.^{5–8} The process for tissue collection and storage has been previously detailed.^{5–8} Briefly, a donor heart is perfused with ice-cold cardioplegic solution, inhibiting contraction and molecular degradation. Samples are then collected and placed into labelled, de-identified cryovials and immediately snap-frozen in liquid nitrogen before

being stored in the Sydney Heart Bank until use. Importantly, this sample is not a post-mortem sample as it was sourced from an aged donor with a noncardiac cause of death, no history of cardiac disease, and had a body mass index (BMI) of less than 30. Furthermore, comprehensive histological investigations confirmed that the sample was taken from a normal heart lacking any pathologies. A single donor heart was used throughout the study to reduce biological variability across experiments. The study protocol adhered to human ethical guidelines, received approval from the Ethics Committee of The University of Sydney (USYD # 2021/122) and was conducted in accordance with the Declaration of Helsinki.

2.2 | Immunohistochemistry (IHC)

2.2.1 | Sample preparation

For sectioning, LV samples were preserved in liquid nitrogen and transferred to a -30°C freezer the day before embedding. Following overnight incubation, samples were then embedded in optimal cutting temperature compound (OCT, Sigma-Aldrich, Melbourne, Australia #SHH0026) and sectioned into $15\ \mu\text{m}$ slices using a cryostat 3000 FSE with the following temperature settings: cryobar at -30°C , chamber at -20°C , and specimen head at -16°C . Sections were then mounted on glass slides (Eprelia, Melbourne, Australia #10149870) and stored for <2 weeks at -30°C until staining.

2.2.2 | Sample selection

To ensure that our sampling was unbiased and representative, we employed a systematic approach to selecting slides taken from different depths of the left ventricle sample. For each experimental condition, we selected adjacent sections for each experimental condition, in order to maintain proximity. We also used sections that were 300 and 600 μm deeper relative to our first set of slides, to gain representative sections at different depths within each LV fragment. This sampling approach ensures that we obtained a representative selection of images.

2.2.3 | Immunostaining

For IF, all incubations were at room temperature (RT) unless stated otherwise. OCT-embedded LV sections were removed from -30°C storage, air-dried for 5 min and fixed for 10, 15, 20 or 30 min with 10% neutral buffered formalin (NBF, Sigma-Aldrich, Melbourne, Australia #HT5012),

-30°C acetone or -30°C methanol. Samples were subsequently washed 3 times for 5 min in phosphate-buffered saline (PBS, Sigma-Aldrich, Melbourne, Australia #SLCH0989) and then incubated in 0.2% (vol/vol) glycine (ThermoFisher, Melbourne, Australia #AJA1083) in PBS for 10 min to chelate any remaining free aldehyde groups and thereby reduce autofluorescence.

Samples were then washed in PBS and NBF-fixed samples were permeabilised with either 0.5% Triton X-100 (Promega, Sydney, Australia #H5141) diluted in PBS or DeepLabel Solution A (DeepLabel Antibody Staining Kit, Logos, Melbourne, Australia #C33001) for 20 min. From this point onwards, the sample wash buffer was either 0.01% TritonX-100 in PBS or, for DeepLabel experiments, DeepLabel wash buffer (DeepLabel Antibody Staining Kit, Logos, Melbourne, Australia #C33001) alone, in a humid chamber. Additionally, all incubations and washes from here onwards were on a rotating platform set at 40 rpm. Samples were washed 3 times for 5 min, then incubated in 5% normal goat serum (NGS; Cell Signalling Technology, Sydney, Australia #5425) and 5% acetylated bovine serum albumin (αBSA ; Sigma-Aldrich, Melbourne, Australia #B8894) in PBS (blocking solution) for 1 h at RT. The samples were then washed 3 times for 5 min and incubated with mouse anti-SERCA2 ATPase (SERCA2; 1:100, Invitrogen Melbourne, Australia #MA3-919), mouse anti- α -actinin-2 (1:50, 20 $\mu\text{g}/\text{mL}$, Sigma-Aldrich, Melbourne, Australia #A7732), anti- α -actinin-2 Affimer (20 $\mu\text{g}/\text{mL}$, made in-house at University of Leeds, UK – see Affimer Synthesis section of the methods for further details) diluted in incubation buffer (0.5% NGS, 0.5% αBSA in 0.01% Triton X-100 PBS) or DeepLabel Solution B (DeepLabel Antibody Staining Kit, Logos, Melbourne, Australia #C33001) overnight at 4°C or for 3 h at RT or 3 h at 37°C . Following incubation, samples were washed 3 times and then incubated with either goat anti-mouse STARGREEN (1:100, Abberior, Göttingen, Germany #STGREEN-1001), goat anti-mouse Alexa Fluor 594 F(ab')₂ (1:200, Invitrogen, Melbourne, Australia #A-11020) or goat anti-mouse Alexa Fluor 594 (1:200, Invitrogen, Melbourne, Australia #A-11032), diluted in incubation buffer or DeepLabel Solution B for 1 h. Subsequently, samples were washed 3 times for 5 min and then incubated with wheat germ agglutinin-647 (WGA-647; 1:200, ThermoFisher, Melbourne, Australia #W32466) diluted in PBS for 1 h. Samples were then washed 3 times for 5 min in PBS or DeepLabel wash buffer and then incubated in DAPI (1 $\mu\text{g}/\text{mL}$ in PBS, Thermo Scientific, Melbourne, Australia #62248,) for 10 min. Finally, coverslips (Carl Zeiss, Sydney, Australia #10474379) were mounted onto samples with Prolong Diamond Antifade Mountant (Invitrogen, Melbourne, Australia #P36961) and then left to cure at RT for 24 h, shielded from light. Samples were then stored at -30°C until imaged.

2.2.4 | Optical clearing and immunostaining

Donor LV tissue was cleared using a modified CUBIC protocol.²³ Briefly, an LV fragment was transferred from liquid nitrogen storage to a -30°C freezer for overnight incubation. The fragment was then incubated in neutral buffered formalin for 24 h at 4°C . Samples were then cut using a microtome blade to approximately $2 \times 8 \times 8$ mm and then immersed in CUBIC Reagent 1A at 37°C for 3 days, with replacement of CUBIC Reagent 1A every 24 h. Samples were then washed 3 times for 1 h in PBS and then permeabilised with DeepLabel Solution A (DeepLabel Antibody Staining Kit, Logos, Melbourne, Australia #C33001) for 1 h. Samples were incubated in blocking solution (5% NGS, 5% α BSA, 0.5% TritonX-100 in PBS) at 4°C overnight. Subsequently, tissue slices were incubated with primary antibodies: mouse anti-SERCA2 (1:50, Invitrogen, Melbourne, Australia #MA3-919), rabbit anti-myomesin 2 (MYOM2; 1:25, Sigma-Aldrich, Melbourne, Australia #HPA001765), rabbit anti-cluster of differentiation 31 (CD31; 1:50, Abcam, Adelaide, Australia #ab281583), and mouse anti-alpha smooth muscle actin (α -SMA; 1:100, Sigma-Aldrich, Melbourne, Australia #a5228), diluted in DeepLabel Solution B or incubation buffer (0.5% NGS, 0.5% α BSA in 0.01% Triton X-100 PBS) for 72 h at RT on a shaker. Samples were then washed 3 times for 30 min with DeepLabel Washing Buffer and then incubated with secondary antibodies goat anti-mouse StarGreen (1:100, Abberior, Göttingen, Germany #STGREEN-1001), goat anti-rabbit Alexa Fluor 594 F(ab')₂ (1:200, Invitrogen, Melbourne, Australia #A-11072) for 2 days on a shaker shielded from light. Tissue was then washed 3 times for 5 min with DeepLabel Washing Buffer, and then incubated with DAPI in PBS for 1 h. Tissue was subsequently washed 3 times for 1 h with DeepLabel Washing Buffer and then cleared with X-Clarity (DeepLabel Antibody Staining Kit, Logos, Melbourne, Australia #C33001) for 1 h. X-Clarity was replaced with fresh X-Clarity and incubated for at least 1 h prior to imaging.

2.2.5 | Affimer synthesis

Affimers targeting the calponin homology (CH) domain of α -actinin-2 were generated as previously described.²⁴ Affimer proteins were then fluorescently conjugated as previously described.²⁵ Briefly, fluorophore labelling of Affimers was performed following elution from the Ni-NTA column. Affimers were diluted to 1.0 mg/mL in PBS before undergoing cysteine activation by incubation with immobilised TCEP (tris(2-carboxyethyl)phosphine) resin (Thermo Fisher) for 1 h at RT. Following this, the sample was clarified at 1000 rpm and the supernatant was extracted and then 100 μM Maleimide-fluorescent

dye stock (STAR 580-maleimide, Abberior, Göttingen, Germany) was added for 2 h at RT. The reaction was then quenched with 1% (v/v) β -mercaptoethanol for 15 min at room temperature. Finally, an equal volume of 80% glycerol was added, and samples were stored at -20°C .

2.2.6 | Epi-fluorescence microscopy

LV tissue stained for IHC was imaged using a Leica Thunder 3D Imager (Leica Microsystems). Images were first acquired using a 10 \times objective (HC PL FLUOTAR, 0.32 NA) via tile-scanning with a 10% overlap. Adjacent tiles were then stitched together using the inbuilt Leica LASX software. Bulb power and exposure time were maintained across all experimental comparisons and samples. Samples were excited at 479 nm with 50% bulb power for 200 ms, and the emission was collected between 507–531 nm.

2.2.7 | Confocal microscopy of slide-mounted samples

LV tissue stained for IHC was imaged using a Leica TCS SP8 STED 3 \times microscope (Leica Microsystems, Australia) in confocal mode. Images were acquired using a 93 \times glycerol objective (HC PL APO, 1.30 NA, #11506417). The fluorophores were excited using either an ultraviolet (UV) laser for DAPI or a tuneable white light laser (WLL). Laser power, laser lines and spectral filters for photomultiplier tubes (PMT) and hybrid detectors (HyD) were configured as follows: DAPI (UV(0.5%), 405^{ex}/416-574^{em}, PMT), StarGreen (WLL(35%), 493^{ex}/503-591^{em}, HyD), Alexa Fluor 594 F(ab')₂ (WLL(21%), 590^{ex}/600-633^{em}, HyD), Abberior STAR580 (WLL(21%), 590^{ex}/600-633^{em}, HyD), Alexa Fluor 594 (WLL(21%), 590^{ex}/600-633^{em}, HyD), WGA-647 (WLL(7%), 650^{ex}/660-781). Images were captured at Nyquist sampling rates and thus to prevent oversampling, axial z-step size varied in accordance with the fluorophore of interest. Thus, for all the slide-mounted confocal images using the StarGreen antibody, the axial z-step size was set to 0.16 μm . For slide-mounted samples utilising either the Alexa Fluor 594 or AbberiorStar580, the step size was set to 0.18 μm . An acquisition speed of 400 Hz accompanied by averaging of 3 line scans was used to acquire images throughout all experiments.

2.2.8 | Confocal imaging of CUBIC cleared samples

CUBIC cleared and IHC stained LV tissue were imaged on glass-bottomed petri dishes (Ibidi, Melbourne, Australia #81158) using a Leica TCS SP8 STED 3 \times microscope set to

confocal mode. The fluorophores were excited using either an ultraviolet (UV) laser for DAPI or a tuneable WLL. Laser lines and spectral filters for PMTs and HyDs were configured differently depending on the experiment, for imaging SERCA2 and MYOM2 the following settings were used: DAPI (UV (56%), 405^{ex}/415-518^{em}, HYD), StarGreen (WLL (56%), 493^{ex}/509-592^{em}, HYD), Alexa Fluor 594 F(ab')₂ (WLL 56%), 590^{ex}/600-676^{em}, HYD). For imaging vascular markers CD31 and α -SMA, the laser intensity was linearly increased to reduce the depth-dependent reduction in fluorescence over 290 microns and used the following settings: DAPI (UV (25-53.2%), 405^{ex}/415-518^{em}, HYD), StarGreen (WLL (27.3-49%), 493^{ex}/509-592^{em}, HYD), Alexa Fluor 594 F(ab')₂ (WLL 8.7-18.5%), 590^{ex}/600-676^{em}, HYD). An acquisition speed of 400 Hz was used to acquire images with 3 line averaging. Axial z-step size was set to 1 μ m for imaging shown in Figure 5, and 2 μ m for imaging as presented in supplementary Figure 4.

2.2.9 | Data analysis

To quantify the fluorescence intensity of low magnification images in human LV tissue samples, we manually performed various image processing steps using FIJI (FIJI is just ImageJ, Version: 2.14.0/1.54f), applied equally to all samples. Initially, nonspecific background fluorescence was subtracted from the images. Subsequently, the images were thresholded to quantify between defined maxima and minima values to outline the sample and eliminate any artefacts from the quantification. Finally, the mean fluorescence intensity was obtained from the thresholded region and was derived using FIJI's inbuilt plugins. For each experiment, samples were imaged once and the sample with the median fluorescence intensity of each group was selected as the representative image. The number of images analysed per experiment are detailed in the corresponding figure legends.

To quantify the fluorescence intensity across the orthogonal projections of the confocal images, we first captured z-stacks of representative areas. Then, taking the orthogonal view, we selected representative regions within each image before using the inbuilt FIJI plugins to plot an intensity profile across the selected region.

Maximum intensity projections were created using FIJI's inbuilt plugins. For each projection, a z-stack of the same distance was defined and maintained throughout an experiment.

Data were plotted as standard error of the mean (SEM) and statistically analysed using a one-way analysis of variance with a Tukey's multiple comparisons post-hoc test. Analysis was performed using GraphPad PRISM version 10 (GraphPad Software, San Diego, CA, USA). Figures were

created with Adobe Illustrator (Adobe Systems Incorporated, San Jose, CA, USA).

3 | RESULTS

During IF of human tissues, considerable unwanted and misleading variation can be observed within the same sample, leading to false positives and negatives. To assess these effects during IF of healthy donor human LV tissue, we examined the interexperimental (technical replicates, performed on separate days) and intraexperimental (technical replicates, performed on the same day) variability. During these experiments, we fixed samples for 15 min with neutral buffered formalin (NBF). This incubation time period was chosen as it falls within the range of 10–30 min seen in the literature.^{26–28} Then, we immunostained for sarco/endoplasmic reticulum calcium ATPase (SERCA2), a target known to have homogeneous expression throughout the healthy LV.²⁹

Using this approach, our results show inter- and intravariability, both visually (Figures 1A and S1A) and quantitatively (Figure 1B). Notably, the intraexperimental variability is less than the interexperimental variability (Figure 1B). Collectively, these findings highlight the importance of only comparing IF experiments conducted on the same day/batch and providing technical replicates to improve accuracy.

To determine the effects of different fixation protocols we performed IF of human LV using NBF, acetone and methanol, for 10, 20 or 30 min. Fixation with acetone increased fluorescence intensity compared to alternative fixatives (Figure 2A and B) but also increased artefactual staining, visible when viewed at high magnification (Figure 2C and D). Conversely, fixation with methanol resulted in the lowest mean fluorescence intensity relative to alternative fixatives (Figure 2A and B), while no method, influenced the fluorescence seen in the no primary control (Figure S1B and C). Although NBF-fixed samples, showed a decreased mean fluorescence intensity relative to acetone fixation, images were relatively free of artefacts, with expected SERCA2 localisation between sarcomeres (Figure 2).³⁰ Due to this observed improved image quality coupled with the relatively low compromise in fluorescence intensity, these results suggest NBF fixation is the preferred fixation method for human LV IF. Furthermore, there were no detectable differences associated with fixation time.

We next assessed the effect of primary antibody incubation at different temperatures: 4°C (control, overnight), room temperature (RT, 3 h) and 37°C (3 h). These results showed that incubating primary antibodies at 37°C significantly increased fluorescence intensity compared to the

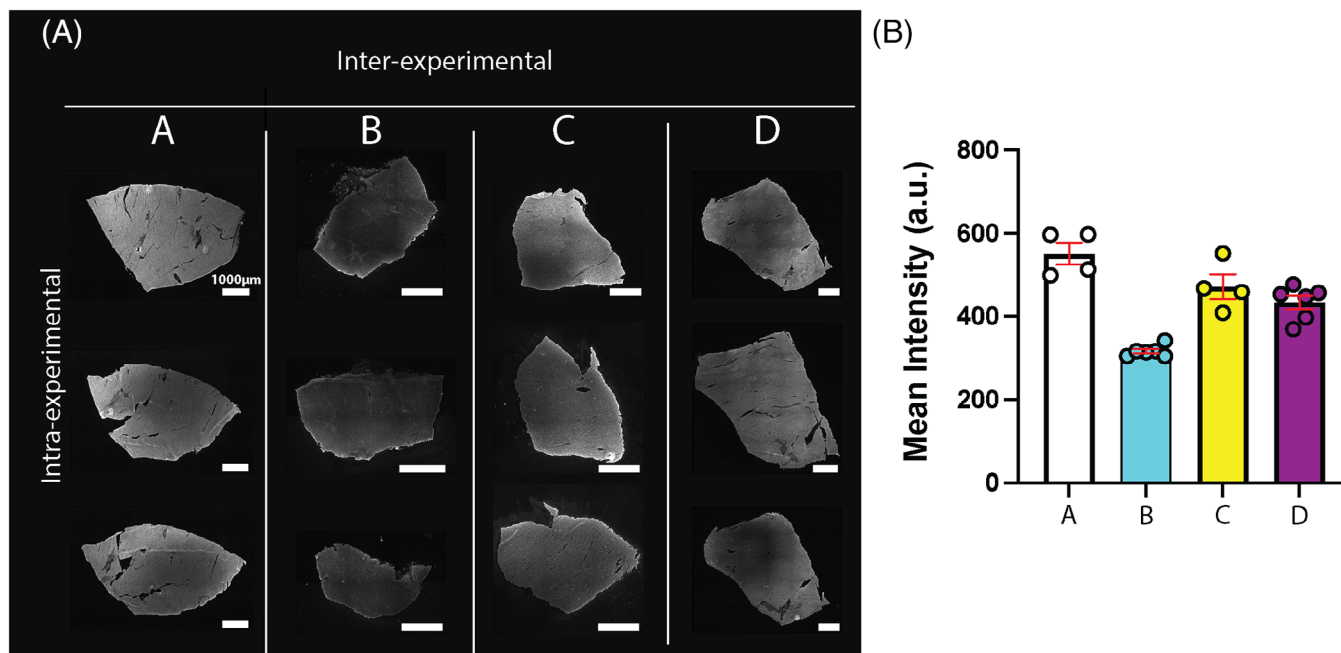


FIGURE 1 Intra- and interexperimental variability in immunofluorescence staining of healthy human left ventricle (LV) tissue. Snap-frozen LV sections (15 μm) from a healthy human donor were fixed with neutral buffered formalin (NBF) for 15 min and then incubated in sarco-/endoplasmic reticulum calcium ATPase (SERCA2) primary antibody overnight at 4°C. (A) Representative immunofluorescence images of the sample, subjected to the same protocol across four distinct experiments conducted on different days (columns), illustrating interexperimental variability. Each column displays 3 technical replicates (median results), illustrating the intraexperimental variability. (B) Quantitative analysis of mean fluorescence intensity in arbitrary units (a.u.) across the four experiments, technical replicates ($n = 4\text{--}6$) are displayed as open circles. Data were presented as mean \pm SEM. Scale bar, 1000 μm .

4°C group (Figure 3A and B). Conversely, incubation at RT was not significantly different from control. Further analysis of the immunostaining quality at higher magnification illustrated that 37°C did not introduce artefacts and produced similar immunostaining patterns as observed in the control (Figure S2).

Next, we performed experiments to explore the potential utility of using techniques derived from thick or whole organ tissue immunofluorescence imaging on thin tissue sections. Specifically, we sought to assess whether DeepLabel reagents could enhance antibody penetration in 15 μm sections. Using this approach, we observed an improvement in antibody penetration in DeepLabel-treated samples relative to untreated controls, as seen in the orthogonal projections and fluorescence intensity measurements along the z -axis (Figure 4A and B). Importantly, treatment of human LV with DeepLabel did not result in artefacts. This finding illustrates DeepLabel can improve antibody penetration in human LV tissue sections.

We also investigated the effect of different methods that aimed to enhance antigen-labelling depth in tissue sections. Specifically, we utilised (1) a primary antibody for the Z-disc marker α -actinin-2 with a fluorescent secondary antibody (control), (2) the same primary antibody with a fragmented fluorescent secondary antibody F(ab')₂, and

(3) a fluorescent targeting α -actinin-2. The stoichiometry of fluorophores linked to Affimers and secondary antibodies differs significantly; Affimers are conjugated with a single fluorophore, whereas secondary antibodies are conjugated with multiple fluorophores. Additionally, multiple polyclonal secondary antibodies (used during these experiments) can bind to the same primary antibody, leading to further signal amplification and varying signal intensities (Figure S3A). To account for these differences and to provide an objective comparison of antibody penetration depth across samples, we maximised image brightness while avoiding pixel saturation at $z = 1.5 \mu\text{m}$ for all samples (Figures 4C and D and S3B). Our findings revealed that the fragmented F(ab')₂ antibody increased signal intensity (Figure 3A) and enhanced labelling depth compared to the regular secondary antibody (Figures 4C and D and S3B). However, while the Affimer-treated samples demonstrated the deepest antigen labelling (as shown in Figures 4C and D and S3B), they exhibited a comparatively weaker fluorescence signal (Figure S3A). In contrast, samples stained with the conventional and F(ab')₂ secondary antibodies displayed high initial signals that diminished with increased depth (Figures 4C and D and S3). These results suggest that both F(ab')₂ and Affimers are effective in improving the visualisation of deeper structures in

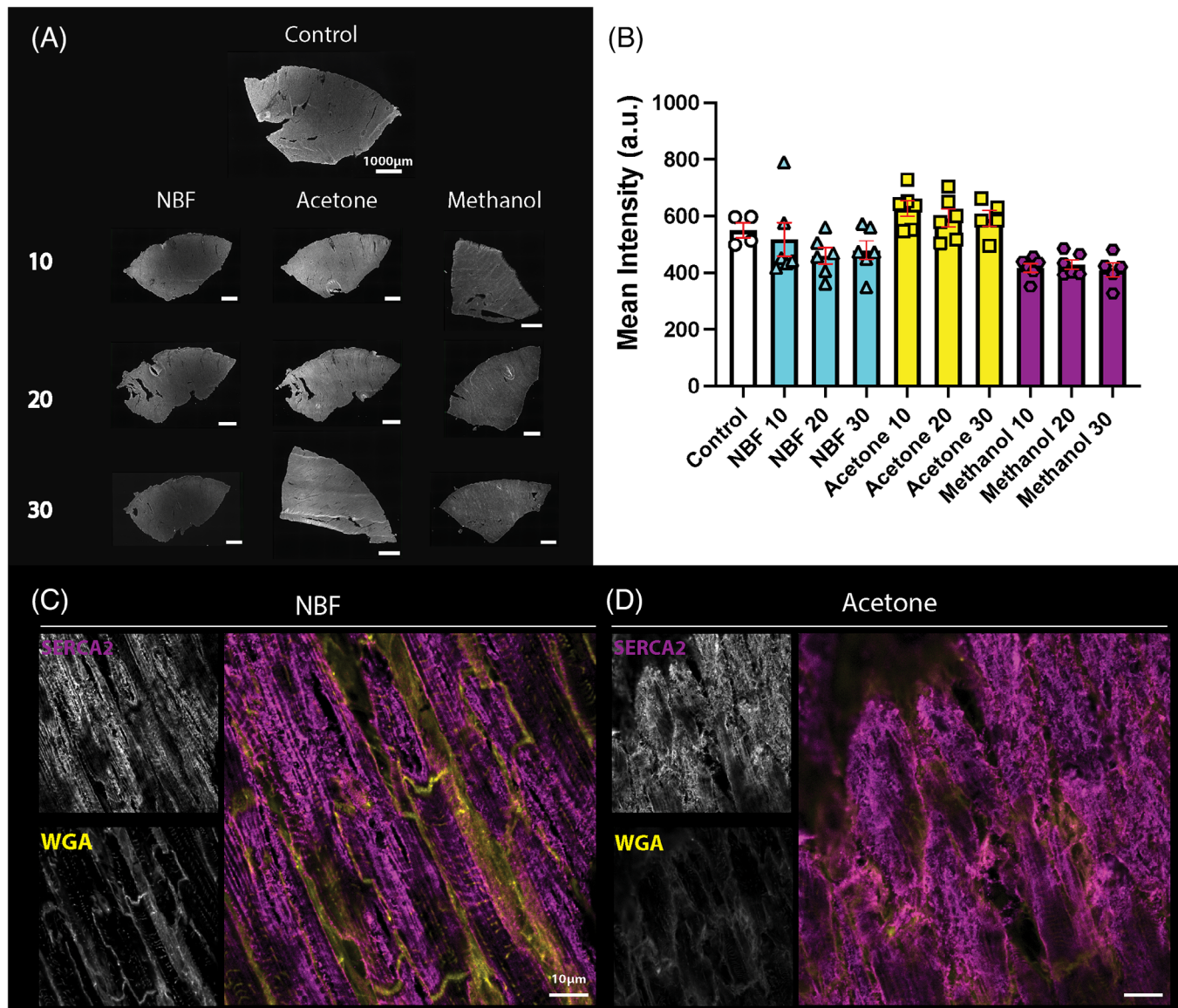


FIGURE 2 Tissue fixation methods effect immunofluorescence staining of healthy human left ventricle (LV) tissue. Snap-frozen LV sections (15 μ m) from a healthy human donor were fixed with neutral buffered formalin (NBF) for 10, 15, 20 or 30 min, -30°C acetone for 10, 20 or 30 min, or -30°C methanol for 10, 20 or 30 min and then incubated in sarco-/endoplasmic reticulum calcium ATPase (SERCA2) primary antibody overnight at 4°C . (A) representative (median) immunofluorescence images from experiments comparing different fixatives (columns) for different fixation durations (rows). Control fixation = 15 min NBF. (B) Quantitative analysis of mean fluorescence intensity in arbitrary units (a.u.) across each fixative and duration, technical replicates ($n = 4\text{--}6$) are displayed as open shapes, data presented as mean \pm SEM. (C) High-magnification image of SERCA2 (grey/magenta) and wheat germ agglutinin (WGA) (grey/yellow) staining in a control sample. (D) High-magnification image of 10-min acetone fixed sample stained with SERCA2 and WGA. Scale bar A = 1000 μ m, C, D = 10 μ m. z-stack thickness 7 μ m.

conventional immunofluorescence studies, with each method presenting distinct advantages in terms of labelling depth and signal intensity.

Thick tissue sections can provide crucial insights into the three-dimensional tissue architecture and cellular distribution to a greater degree than thin tissue sections, thus enabling a more comprehensive understanding of the spatial relationships within the tissue. Despite these advantages, obtaining high-quality images from thick tis-

sue sections is challenging. The primary challenges are the inability of antibodies sufficiently penetrate the tissue and the increased light scattering that accompanies thicker tissue. Thus, following the findings in thin tissue sections, we investigated whether DeepLabel could improve antibody penetration in thick (approximately 2–3 mm) optically cleared (CUBIC) human LV tissue fragments (Figure 5A). DeepLabel-treated samples exhibited comparable staining patterns to that observed in thin tissue

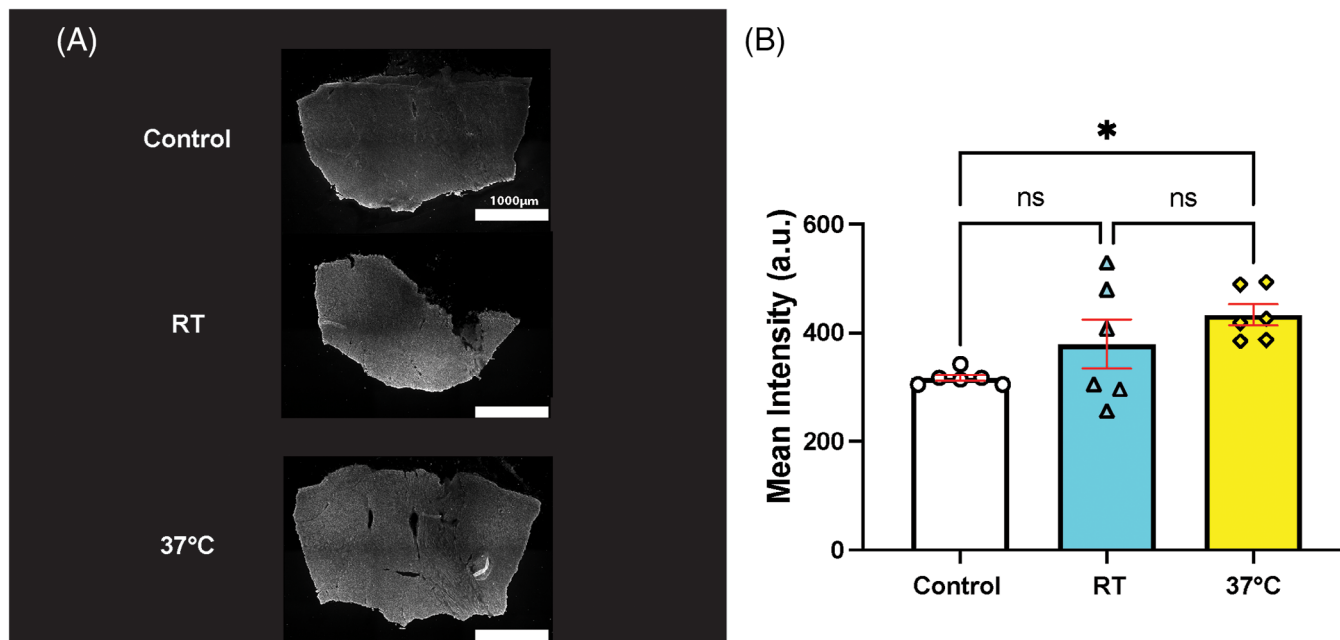


FIGURE 3 Primary antibody incubation temperatures effect immunofluorescence staining of healthy human left ventricle (LV) tissue. Snap-frozen LV sections (15 μm) from a healthy human donor were fixed with neutral buffered formalin (NBF) for 15 min and incubated in sarco-/endoplasmic reticulum calcium ATPase (SERCA2, grey) primary antibody overnight at 4°C (control), 3 h at room temperature (RT) or 3 h at 37°C. (A) Representative (median) immunofluorescence images, scale bars = 1000 μm. (B) Quantitative image analysis of the mean fluorescence intensity in arbitrary units (a.u.), technical replicates ($n = 6$) represented as open shapes, error bars presented as mean ± SEM and statistically analysed by a one-way analysis of variance with a Tukey's multiple comparisons test (* $p < 0.05$, ns = not significant).

sections (Figure 5B). Penetration of antibodies was improved by DeepLabel and is demonstrated with the orthogonal views (Figure 5B). In addition to cardiomyocytes markers SERCA2 and MYOM2, we also compared antibody penetration of endothelial marker cluster of differentiation 31 (CD31) and smooth muscle cell/myofibroblast marker α -smooth muscle actin (α SMA) (Figure S4). Consistent with the results observed for SERCA2 and MYOM2, we observed improved antibody penetration with DeepLabel (Figure S4). No primary controls confirmed the specificity for all our antibodies with and without DeepLabel (Figure S1C and D). These findings establish that LV tissue fragments can be utilised to perform immunostaining and that DeepLabel can enhance antibody penetration.

4 | DISCUSSION

In this study, we systematically compared IF techniques using donor human cardiac tissues with the aim to improve biological reproducibility, increase fluorescence signal, and minimise artefacts. We first demonstrated significant intra- and interexperimental variability, demonstrating the importance of conducting IF experiments within the same batch and including technical replicates

to improve accuracy. We next showed that fixing frozen LV tissue for 15 min with NBF generated artefact-free and sufficient fluorescent signal as compared to other fixation methods. Moreover, our findings indicated that antibody incubation at approximately human body temperature improved fluorescence intensity without introducing artefacts, compared to the conventional 4°C incubation. Finally, we investigated tools and reagents to promote antibody penetration and labelling depth. This showed that antibody and label penetration were improved by DeepLabel, fragmented antibodies and Affimers. Collectively, these optimised conditions established a systematic approach for IF imaging in human cardiac tissue.

Variations in immunostaining intensity between different slides and batches represent potential sources of experimental error, with previous studies showing a clear inter- and intraexperimental variability in IHC staining.^{10–12} However, to the best of our knowledge such variation has not been shown in human LV tissue staining. Thus, using the abundantly and homogeneously expressed cardiomyocyte marker SERCA2,^{29,31} we showed while there is intraexperimental variability (same sample, same batch) in staining intensity, it is less than the interexperimental variation (same sample, different batch) that we observed. A potential explanation for the observed interexperimental variation is the length of the IHC protocol introduces

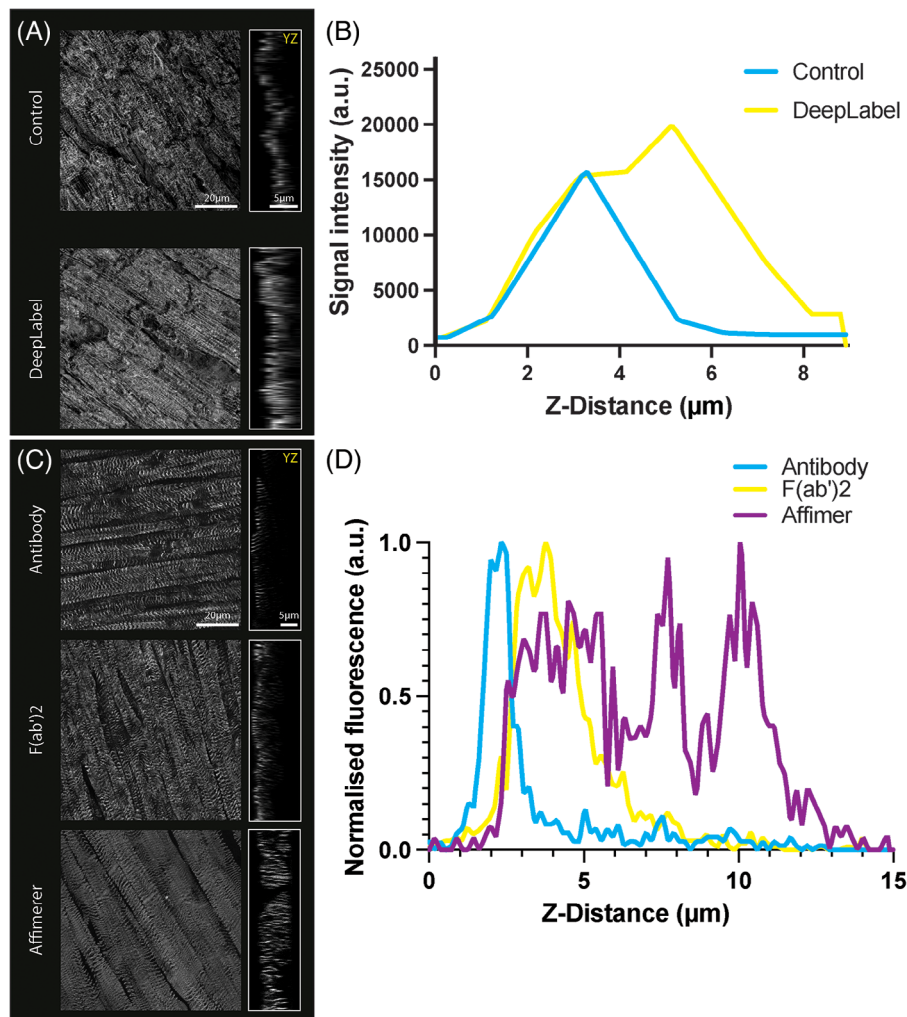


FIGURE 4 DeepLabel, fragmented antibodies and Affimers improve penetration in healthy human left ventricle (LV) tissue sections. Snap-frozen LV sections (15 µm) from a healthy human donor were fixed with neutral buffered formalin (NBF) for 15 min and processed \pm DeepLabel. Samples were then incubated with antibodies targeting either sarco-/endoplasmic reticulum calcium ATPase (SERCA2) or α -actinin-2, or with Affimers targeting α -actinin-2, overnight at 4°C. (A) Representative maximum intensity projections of SERCA2 \pm DeepLabel (scale bar = 20 µm), adjacent to each image is its corresponding orthogonal (YZ) projection (scale bars = 5 µm). (B) Signal intensity profiles of SERCA2 \pm DeepLabel in arbitrary units (a.u.) across the YZ-axis. (C) Representative maximum intensity projections for antibody, F(ab')2 and Affimer experiments targeting α -actinin-2 (scale bar = 20 µm), adjacent to each image is its corresponding orthogonal (YZ) projection (scale bars = 5 µm), brightness and contrast were optimised to the $z = 1.5$ µm slice of each sample and propagated through each z-stack. (D) Normalised signal intensity profiles in arbitrary units (a.u.) of antibody, F(ab')2 and Affimer targeting α -actinin-2 across the YZ-axis. Signal intensities were normalised to the maximum fluorescence intensity of each YZ projection. All images are representative of 6 technical replicates. z-stack thickness = 9 and 15 µm for images in A and C.

numerous opportunities for error together with small environmental differences in laboratory temperature and humidity. Therefore, our results show that staining all slides for an experiment on the same day and averaging multiple technical replicates for consistency is recommended.

Fixatives play a crucial role in immunofluorescence studies by stabilising the tissue architecture and preserving the native arrangement of proteins.⁴ Importantly, different fixatives preserve the cellular and subcellular architecture through different mechanisms, which can

result in differences in tissue preservation and overall staining.⁴ Thus, the choice of fixative affects not only the structural integrity of the tissue sample, but also the accessibility and presence of antigens during immunostaining.⁴ Studies have demonstrated that fixing rat cardiac myofibroblasts and mouse skeletal muscle tissue with acetone or methanol, which precipitate proteins, can preserve the antigenicity of proteins more effectively than aldehydes.^{32,33} However, acetone and methanol have also been found to disrupt membrane integrity in MDCK cells, MCF-7 cells and liver sinusoidal endothelial cells,

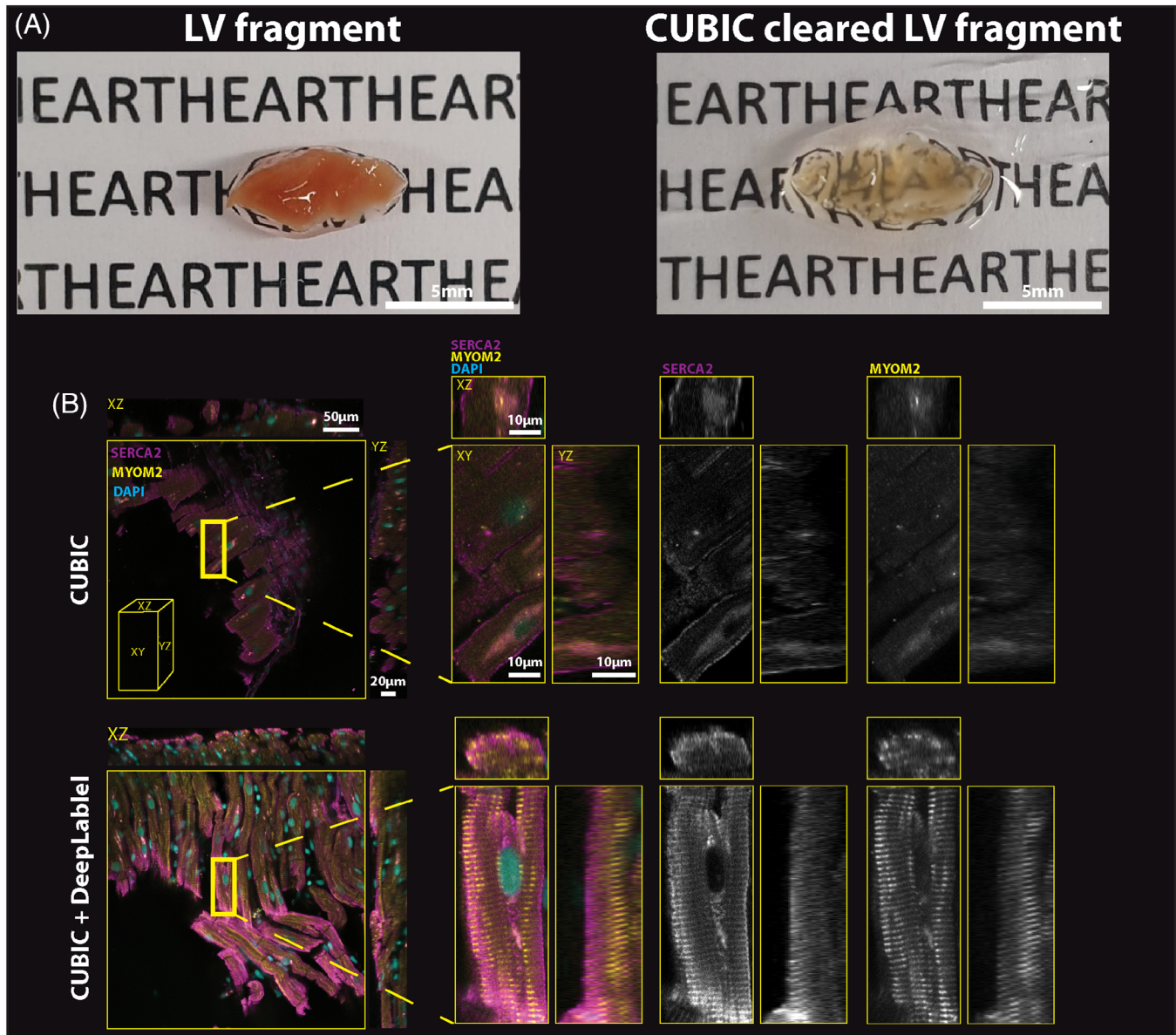


FIGURE 5 DeepLabel improves visualisation of optically cleared healthy human left ventricle (LV) tissue fragments. LV fragments underwent CUBIC clearing \pm DeepLabel and immunostained with antibodies targeting sarco-/endoplasmic reticulum calcium ATPase (SERCA2, grey/magenta), myomesin-2 (MYOM2, grey/yellow), and 4',6-diamidino-2-phenylindole (DAPI, cyan). (A) Representative photo of control (uncleared) versus CUBIC cleared LV fragments (scale bars = 5 mm). (B) Representative confocal images of CUBIC cleared LV fragments \pm DeepLabel (XY scale bar = 50 μm , orthogonal projections scale bars XZ = 50 μm and YZ = 20 μm respectively). Insets of regions in (B, CUBIC + DeepLabel) indicated by yellow rectangle (scale bars = 10 μm). Each image is representative of 5 technical replicates. z-stack thickness = 52 μm .

leading to redistribution and removal of proteins and lipids from the cytosol.^{3,34,35} Our findings are therefore in agreement with previous work as we have shown that fixing with methanol results in a lower fluorescence signal, which would be consistent with the extraction of protein from the tissue. Additionally, fixing with acetone may enhance SERCA2 antigenicity while it may also disrupt membrane integrity and lead to the redistribution of SERCA2, resulting in our observed artefactual stain-

ing. In contrast, we showed that NBF, which fixes tissue by creating intra- and intermolecular cross-links between side chain amino groups, yielded adequate and characteristic SERCA2 staining.^{30,36} The cross-linking activity of NBF anchors proteins in their native location without perturbing cellular organelles thus resulting in the characteristic SERCA2 staining pattern, a finding consistent with numerous studies demonstrating that formalin sufficiently preserves most proteins.^{27,36} A caveat of NBF is that the

formation of cross-links can mask epitopes of target antigens and thereby reduce antigenicity which is a common limitation encountered in formalin-fixed paraffin-embedded tissue, and may account for the marginally lower fluorescence signal observed in the NBF-treated group relative to acetone.³⁶ These findings highlight the effect of fixation on the quality and intensity of immunofluorescence staining and further illustrate the importance of selecting an appropriate fixative to preserve your target of interest.

Historically, primary antibody incubation temperatures of 4°C or room temperature (approximately 21°C) have been employed for IF/IHC.³⁷ Our findings indicated that incubating healthy human donor LV thin tissue sections with primary antibodies at 37°C (a temperature similar to physiological mammalian core body temperatures³⁸) enhanced the fluorescence signal. This is consistent with work conducted using thick tissue sections.^{13,39–44} Specifically, studies using intraaxonal and astrocytic markers conducted on free-floating skin, peripheral nerve and spinal cord thick tissue sections has demonstrated that incubation at 37°C can improve immunofluorescence staining by increasing the intensity and contrast of biological structures.¹³ Additionally, protocols designed for immunostaining optically cleared thick tissue sections or entire organs, such as iDISCO, CUBIC, ScaleS and Clarity, also routinely employ antibody incubations at 37°C in order to improve antibody penetration and staining.^{39–44} A possible explanation for this improvement is that incubating primary antibodies at 37°C facilitates antibody-antigen interactions by increasing antibody kinetic energy and thereby the mobility of antibodies.^{13,45} This would be consistent with work conducted on the mouse brain which demonstrated that incubation at 37°C improved the diffusion of FITC-conjugated dextran, relative to incubation at 4°C.⁴⁵ These results emphasise the importance of antibody incubation temperatures on immunofluorescence staining and further illustrate that techniques or concepts employed in thick tissue staining are also beneficial for IHC protocols in thin cardiac tissue sections.

Antibody penetration is critical for optimal imaging of deep structures within tissue sections. This can be challenging in dense cardiac tissue as traditional antibody staining techniques are unable to penetrate and label deep into the tissue.⁴⁶ To address this problem, we compared F(ab')₂ and Affimers to traditional antibodies, showing their superiority for deeper visualisation of cardiomyocyte structures. Our findings that Affimers (~10–12 kDa) penetrate the deepest, followed by F(ab')₂ (~110 kDa) and finally conventional antibodies (~150 kDa), are consistent with the understanding that penetration depth is inversely proportional to the size of the probe.^{17,19,20,47} This has been previously demonstrated using nanobod-

ies, which are similarly small antibodies (~10–15 kDa) that certain cartilaginous fish and camelids naturally create.^{17,18} Additionally, due to their smaller size, Affimers and F(ab')₂ also provide improved resolution as they are closer to the target of interest.¹⁸ These findings indicate that smaller probes, such as fragmented antibodies and Affimers, enable deeper labelling of subcellular structures compared to regularly employed secondary antibodies in LV tissue. Thus, smaller probes may enable improved visualisation and characterisation of subcellular structures of LV tissue.

In our experiments, treating samples with DeepLabel increased the antibody penetration of all markers in both thin and CUBIC optically cleared thick tissue fragments. While the finding that DeepLabel improves antibody penetration in thick tissue sections has been previously described,¹⁶ its similar effect on thin cardiac tissue sections, as shown here, is an important finding as it illustrates another means of improving labelling depth in conventional microscopy. Interestingly, we found that the antibodies against MYOM2 and SERCA2, abundantly expressed proteins in cardiomyocytes, exhibited less tissue penetration than antibodies targeting the vascular markers CD31 and α -SMA. These findings are consistent with the notion that antibody penetration is inversely related to the concentration of the target epitope, which has been previously demonstrated.⁴² Additionally, the increase in penetration of the vascular markers may have been facilitated by the vessel lumen that may provide a tubular system that reduces antibody diffusion requirements. These findings underscore the potential of DeepLabel as a tool for enhancing antibody penetration in cardiac tissue, which is particularly useful for high-resolution three-dimensional bioimaging.

Given that this study only utilised fresh-frozen LV tissue for its optimisation, the generalisability of these findings to other section types used for IHC, including paraffin-embedded sections, may be limited. Similarly, the generalisability of our results directly to diseased heart tissue, such as infarcted tissue, may be limited as the current workflow may not adequately address the heterogeneous necrotic areas and increased extracellular matrix deposition. Further studies need to be undertaken to explore the distinct demands of each of these states. Additionally, the use of a single sample, although minimising biological variability, limits our ability to assess the reproducibility of our findings across different age ranges and demographics. Other limitations include that the study did not extend itself to all variables of the IHC protocol, such as alternative permeabilisation and blocking methods which could significantly influence antibody accessibility and binding, and thus will be explored in future studies. Notwithstanding these limitations, this study showcases a variety of

approaches that may be undertaken to improve the quality of microscopy images.

In conclusion, this study has made significant findings that contribute to the optimisation of IF techniques for fresh-frozen cardiac tissue, improving biological reproducibility, increasing fluorescence signal, and minimising artefacts. This study demonstrated the significant experimental variability in fluorescence staining of human LV tissue and two enhancements including fixation and incubation temperatures, as well as various methods to improve antibody penetration and labelling depth. Collectively, these findings contribute to a more accurate visualisation of the intricate 3D architecture of the human myocardium, thus providing cardiac researchers with easily accessible alternative IF protocols for improved imaging and analyses.

ACKNOWLEDGEMENTS

We thank the patients and staff of St Vincent's Hospital, Sydney, and the Australian Red Cross Blood Service. This was supported by the R.T. Hall Trust and The Baird Institute. The Sydney Heart Bank Human Ethics Approval number is 2021/122. We would also like to acknowledge the facilities at the Australian Microscopy and Microanalysis Research Facility at Sydney Microscopy and Microanalysis, University of Sydney, as well as the technical assistance provided by Dr. Neftali Rodriguez and Dr. Ying Ying Su.

Open access publishing facilitated by The University of Sydney, as part of the Wiley - The University of Sydney agreement via the Council of Australian University Librarians.

CONFLICT OF INTEREST STATEMENT

The authors declare no conflicts of interest.

ORCID

Matthew Taper  <https://orcid.org/0000-0002-3148-1615>

Michelle Peckham  <https://orcid.org/0000-0002-3754-2028>

2028

Robert D. Hume  <https://orcid.org/0000-0003-3694-9333>

REFERENCES

- Kolesova, H., Olejnickova, V., Kvasilova, A., Gregorovicova, M., & Sedmera, D. (2021). Tissue clearing and imaging methods for cardiovascular development. *IScience*, *24*(4), 102387.
- Taatjes, D. J., Wadsworth, M. P., Quinn, A. S., Rand, J. H., Bovill, E. G., & Sobel, B. E. (2008). Imaging aspects of cardiovascular disease at the cell and molecular level. *Histochemistry and Cell Biology*, *130*(2), 235–245.
- Schnell, U., Dijk, F., Sjollem, K. A., & Giepmans, B. N. (2012). Immunolabeling artifacts and the need for live-cell imaging. *Nature Methods*, *9*(2), 152–158.
- Im, K., Mareninov, S., Diaz, M. F. P., & Yong, W. H. (2019). An introduction to performing immunofluorescence staining. *Methods in Molecular Biology*, *1897*, 299–311.
- Zhu, Y., Jackson, D., Hunter, B., Beattie, L., Turner, L., Hambly, B. D., Jeremy, R. W., Malecki, C., Robertson, E. N., Li, A., Dos Remedios, C., Richmond, D., Semsarian, C., O'Sullivan, J. F., Bannon, P. G., & Lal, S. (2022). Models of cardiovascular surgery biobanking to facilitate translational research and precision medicine. *ESC Heart Failure*, *9*(1), 21–30.
- Lal, S., Li, A., Allen, D., Allen, P. D., Bannon, P., Cartmill, T., Cooke, R., Farnsworth, A., Keogh, A., & Dos Remedios, C. (2015). Best practice BioBanking of human heart tissue. *Biophysical Reviews*, *7*(4), 399–406.
- Li, M., Parker, B. L., Pearson, E., Hunter, B., Cao, J., Koay, Y. C., Guneratne, O., James, D. E., Yang, J., Lal, S., & O'Sullivan, J. F. (2020). Core functional nodes and sex-specific pathways in human ischaemic and dilated cardiomyopathy. *Nature Communications*, *11*(1), 2843.
- Dos Remedios, C. G., Lal, S. P., Li, A., McNamara, J., Keogh, A., Macdonald, P. S., Cooke, R., Ehler, E., Knoll, R., Marston, S. B., Stelzer, J., Granzier, H., Bezzina, C., van Dijk, S., De Man, F., Stienen, G. J. M., Odeberg, J., Ponten, F., Linke, W. A., ... van der Velden, J. (2017). The Sydney Heart Bank: Improving translational research while eliminating or reducing the use of animal models of human heart disease. *Biophysical Reviews*, *9*(4), 431–441.
- Coppola, L., Cianflone, A., Grimaldi, A. M., Incoronato, M., Bevilacqua, P., Messina, F., Baselice, S., Soricelli, A., Mirabelli, P., & Salvatore, M. (2019). Biobanking in health care: Evolution and future directions. *Journal of Translational Medicine*, *17*(1), 172.
- Stopsack, K. H., Tyekucheva, S., Wang, M., Gerke, T. A., Vaselkiv, J. B., Penney, K. L., Kantoff, P. W., Finn, S. P., Fiorentino, M., Loda, M., Lotan, T. L., Parmigiani, G., & Mucci, L. A. (2021). Extent, impact, and mitigation of batch effects in tumor biomarker studies using tissue microarrays. *Elife*, *10*, e71265.
- Chang, Y. H., Chin, K., Thibault, G., Eng, J., Burlingame, E., & Gray, J. W. (2020). RESTORE: Robust intEnSiTy nORmalization mEthod for multiplexed imaging. *Communications Biology*, *3*(1), 111.
- Johnsson, A., Olsson, C., Anderson, H., & Cavallin-Stahl, E. (1994). Evaluation of a method for quantitative immunohistochemical analysis of cisplatin-DNA adducts in tissues from nude mice. *Cytometry*, *17*(2), 142–150.
- Xiao, X., Feng, Y. P., Du, B., Sun, H. R., Ding, Y. Q., & Qi, J. G. (2017). Antibody incubation at 37 degrees C improves fluorescent immunolabeling in free-floating thick tissue sections. *Biotechniques*, *62*(3), 115–122.
- Zaglia, T., Di Bona, A., Chioato, T., Basso, C., Ausoni, S., & Mongillo, M. (2016). Optimized protocol for immunostaining of experimental GFP-expressing and human hearts. *Histochemistry and Cell Biology*, *146*(4), 407–419.
- Mochama, P., Tyshynsky, R., & Sanders, M. A. (2019). Multiplex immunolabeling and imaging of functionally essential kidney structures in X-CLARITY-cleared tissue. *Microscopy and Microanalysis*, *25*(S2), 1260–1261.
- Kim, M. S., Ahn, J. H., Mo, J. E., Song, H. Y., Cheon, D., Yoo, S. H., & Choi, H. J. (2021). Optimizing tissue clearing and

- imaging methods for human brain tissue. *Journal of International Medical Research*, 49(3), 3000605211001729.
17. Fang, T., Lu, X., Berger, D., Gmeiner, C., Cho, J., Schalek, R., Ploegh, H., & Lichtman, J. (2018). Nanobody immunostaining for correlated light and electron microscopy with preservation of ultrastructure. *Nature Methods*, 15(12), 1029–1032.
 18. Carrington, G., Tomlinson, D., & Peckham, M. (2019). Exploiting nanobodies and Affimers for superresolution imaging in light microscopy. *Molecular Biology of the Cell*, 30(22), 2737–2740.
 19. Tiede, C., Bedford, R., Heseltine, S. J., Smith, G., Wijetunga, I., Ross, R., AlQallaf, D., Roberts, A. P., Balls, A., Curd, A., Hughes, R. E., Martin, H., Needham, S. R., Zanetti-Domingues, L. C., Sadigh, Y., Peacock, T. P., Tang, A. A., Gibson, N., Kyle, H., ... Tomlinson, D. C. (2017). Affimer proteins are versatile and renewable affinity reagents. *Elife*, 6, e24903.
 20. Bates, A., & Power, C. A. (2019). David vs. Goliath: The structure, function, and clinical prospects of antibody fragments. *Antibodies (Basel)*, 8(2), 28.
 21. Borlaug, B. A., Sharma, K., Shah, S. J., & Ho, J. E. (2023). Heart failure with preserved ejection fraction: JACC scientific statement. *Journal of the American College of Cardiology*, 81(18), 1810–1834.
 22. Murphy, S. P., Ibrahim, N. E., & Januzzi, J. L. Jr (2020). Heart failure with reduced ejection fraction: A review. *Jama*, 324(5), 488–504.
 23. Lloyd-Lewis, B., Davis, F. M., Harris, O. B., Hitchcock, J. R., Lourenco, F. C., Pasche, M., & Watson, C. J. (2016). Imaging the mammary gland and mammary tumours in 3D: optical tissue clearing and immunofluorescence methods. *Breast Cancer Research*, 18(1), 127.
 24. Curd, A. P., Leng, J., Hughes, R. E., Cleasby, A. J., Rogers, B., Trinh, C. H., Baird, M. A., Takagi, Y., Tiede, C., Sieben, C., Manley, S., Schlichthaerle, T., Jungmann, R., Ries, J., Shroff, H., & Peckham, M. (2021). Nanoscale pattern extraction from relative positions of sparse 3D localizations. *Nano Letters*, 21(3), 1213–1220.
 25. Schlichthaerle, T., Eklund, A. S., Schueder, F., Strauss, M. T., Tiede, C., Curd, A., Ries, J., Peckham, M., Tomlinson, D. C., & Jungmann, R. (2018). Site-specific labeling of affimers for DNA-PAINT microscopy. *Angewandte Chemie (International ed in English)*, 57(34), 11060–11063.
 26. Sun, T., Grassam-Rowe, A., Pu, Z., Li, Y., Ren, H., An, Y., Guo, X., Hu, W., Liu, Y., Zheng, Y., Liu, Z., Kou, K., Ou, X., Chen, T., Fan, X., Liu, Y., Tu, S., He, Y., Ren, Y., ... Lei, M. (2023). Dbh(+) catecholaminergic cardiomyocytes contribute to the structure and function of the cardiac conduction system in murine heart. *Nature Communications*, 14(1), 7801.
 27. Shi, S. R., Liu, C., Pootrakul, L., Tang, L., Young, A., Chen, R., Cote, R. J., & Taylor, C. R. (2008). Evaluation of the value of frozen tissue section used as “gold standard” for immunohistochemistry. *American Journal of Clinical Pathology*, 129(3), 358–366.
 28. Jin, Y., Kim, H., Min, S., Choi, Y. S., Seo, S. J., Jeong, E., Kim, S. K., Lee, H. A., Jo, S. H., Park, J. H., Park, B. W., Sim, W. S., Kim, J. J., Ban, K., Kim, Y. G., Park, H. J., & Cho, S. W. (2022). Three-dimensional heart extracellular matrix enhances chemically induced direct cardiac reprogramming. *Science Advances*, 8(50), eabn5768.
 29. Krishnan, B., Massilamany, C., Basavalingappa, R. H., Gangaplara, A., Rajasekaran, R. A., Afzal, M. Z., Khalilzad-Sharghi, V., Zhou, Y., Riethoven, J. J., Nandi, S. S., Mishra, P. K., Sobel, R. A., Strande, J. L., Steffen, D., & Reddy, J. (2018). Epitope mapping of SERCA2a identifies an antigenic determinant that induces mainly atrial myocarditis in A/J mice. *Journal of Immunology*, 200(2), 523–537.
 30. Dally, S., Bredoux, R., Corvazier, E., Andersen, J. P., Clausen, J. D., Dode, L., Fanchaouy, M., Gelebart, P., Monceau, V., Del Monte, F., Gwathmey, J. K., Hajjar, R., Chaabane, C., Bobe, R., Raies, A., & Enouf, J. (2006). Ca²⁺-ATPases in non-failing and failing heart: evidence for a novel cardiac sarco/endoplasmic reticulum Ca²⁺-ATPase 2 isoform (SERCA2c). *Biochemical Journal*, 395(2), 249–258.
 31. Periasamy, M., Bhupathy, P., & Babu, G. J. (2008). Regulation of sarcoplasmic reticulum Ca²⁺ ATPase pump expression and its relevance to cardiac muscle physiology and pathology. *Cardiovascular Research*, 77(2), 265–273.
 32. Smith-Clerc, J., & Hinz, B. (2010). Immunofluorescence detection of the cytoskeleton and extracellular matrix in tissue and cultured cells. *Methods in Molecular Biology*, 611, 43–57.
 33. Rogers, G. L., & Hoffman, B. E. (2012). Optimal immunofluorescent staining for human factor IX and infiltrating T cells following gene therapy for hemophilia B. *Journal of Genetic Syndromes & Gene Therapy*, 51, 012.
 34. Hoetelmans, R. W., Prins, F. A., Cornelese-ten Velde, I., van der Meer, J., van de Velde, C. J., & van Dierendonck, J. H. (2001). Effects of acetone, methanol, or paraformaldehyde on cellular structure, visualized by reflection contrast microscopy and transmission and scanning electron microscopy. *Applied Immunohistochemistry & Molecular Morphology*, 9(4), 346–351.
 35. Vekemans, K., Rosseel, L., Wisse, E., & Braet, F. (2004). Immuno-localization of Fas and FasL in rat hepatic endothelial cells: influence of different fixation protocols. *Micron (Oxford, England: 1993)*, 35(4), 303–306.
 36. Sompuram, S. R., Vani, K., Messana, E., & Bogen, S. A. (2004). A molecular mechanism of formalin fixation and antigen retrieval. *American Journal of Clinical Pathology*, 121(2), 190–199.
 37. Zaqout, S., & Becker, L. L., & Kaindl, A. M. (2020). Immunofluorescence staining of paraffin sections step by step. *Frontiers in Neuroanatomy*, 14, 582218.
 38. Mota-Rojas, D., Titto, C. G., Orihuela, A., Martinez-Burnes, J., Gomez-Prado, J., Torres-Bernal, F., Flores-Padilla, K., Carvajal-de la Fuente, V., & Wang, D. (2021). Physiological and behavioral mechanisms of thermoregulation in mammals. *Animals (Basel)*, 11(6), 1733.
 39. Zheng, H., & Rinaman, L. (2016). Simplified CLARITY for visualizing immunofluorescence labeling in the developing rat brain. *Brain Structure and Function*, 221(4), 2375–2383.
 40. Lai, H. M., Liu, A. K. L., Ng, H. H. M., Goldfinger, M. H., Chau, T. W., DeFelice, J., Tilley, B. S., Wong, W. M., Wu, W., & Gentleman, S. M. (2018). Next generation histology methods for three-dimensional imaging of fresh and archival human brain tissues. *Nature Communications*, 9(1), 1066.
 41. Nojima, S., Susaki, E. A., Yoshida, K., Takemoto, H., Tsujimura, N., Iijima, S., Takachi, K., Nakahara, Y., Tahara, S., Ohshima, K., Kurashige, M., Hori, Y., Wada, N., Ikeda, J. I., Kumanogoh, A., Morii, E., & Ueda, H. R. (2017). CUBIC pathology:

- Three-dimensional imaging for pathological diagnosis. *Scientific Reports*, 7(1), 9269.
42. Liu, A. K., Hurry, M. E., Ng, O. T., DeFelice, J., Lai, H. M., Pearce, R. K., Wong, G. T., Chang, R. C., & Gentleman, S. M. (2016). Bringing CLARITY to the human brain: visualization of Lewy pathology in three dimensions. *Neuropathology and Applied Neurobiology*, 42(6), 573–587.
43. Xu, N., Tamadon, A., Liu, Y., Ma, T., Leak, R. K., Chen, J., Gao, Y., & Feng, Y. (2017). Fast free-of-acrylamide clearing tissue (FACT)—an optimized new protocol for rapid, high-resolution imaging of three-dimensional brain tissue. *Scientific Reports*, 7(1), 9895.
44. Renier, N., Wu, Z., Simon, D. J., Yang, J., Ariel, P., & Tessier-Lavigne, M. (2014). iDISCO: A simple, rapid method to immunolabel large tissue samples for volume imaging. *Cell*, 159(4), 896–910.
45. Gleave, J. A., Lerch, J. P., Henkelman, R. M., & Nieman, B. J. (2013). A method for 3D immunostaining and optical imaging of the mouse brain demonstrated in neural progenitor cells. *PLoS ONE*, 8(8), e72039.
46. Nehrhoff, I., Bocancea, D., Vaquero, J., Vaquero, J. J., Ripoll, J., Desco, M., & Gomez-Gaviro, M. V. (2016). 3D imaging in CUBIC-cleared mouse heart tissue: going deeper. *Biomedical Optics Express*, 7(9), 3716–3720.
47. Tiede, C., Tang, A. A., Deacon, S. E., Mandal, U., Nettleship, J. E., Owen, R. L., George, S. E., Harrison, D. J., Owens, R. J., Tomlinson, D. C., & McPherson, M. J. (2014). Adhiron: A stable and versatile peptide display scaffold for molecular recognition applications. *Protein Engineering, Design and Selection*, 27(5), 145–155.

SUPPORTING INFORMATION

Additional supporting information can be found online in the Supporting Information section at the end of this article.

How to cite this article: Taper, M., Carrington, G., Peckham, M., Lal, S., & Hume, R. D. (2024). A comparison of fixation and immunofluorescence protocols for successful reproducibility and improved signal in human left ventricle cardiac tissue. *Journal of Microscopy*, 1–14.
<https://doi.org/10.1111/jmi.13336>